Supplementary Information

Bond elasticity controls molecular recognition specificity in antibody-antigen binding

Anna Alemany[1], Nuria Sanvicens[2,3], Sara de Lorenzo[1], M.-Pilar Marco[2,3], Felix Ritort[1,3,*]

[1]Small Biosystems Lab, Departament de Física Fonamental, Universitat de Barcelona. C/ Martí i Franquès 1, 08028 Barcelona, Spain; [2]Nanobiotechnology for Diagnostics (Nb4D) group, Centro Superior de Investigaciones Científicas, C/ Jordi Girona 18-26, 08034 Barcelona, Spain; and [3] Networking Research Center of Bioengineering, Biomaterials and Nanomedicine (CIBER-BBN), Instituto Carlos III, C/ Sinesio Delgado 4, 28029 Madrid, Spain; * Corresponding author: e-mail: ritort@ub.edu; phone: +34-934035869; fax: +34-934021149

Contents

S1 Antibody/antigen conjugation to polystyrene beads

Carboxy-derivatized polystyrene beads of 3 μm and 2 μm diameter (Kisker Biotech GmbH & Co., Germany) were used for conjugation of antibody and antigen, respectively. Beads (250 μl/sample) were washed twice with 1 ml of 10 mM NaH_2PO_4, pH 6 (buffer A). Following centrifugation at 10000 rpm for 5 min, beads were resuspended in 1 m1 of buffer A. Then, 2.5 ml of a 90 mM solution of N-(3-dimethylaminopropyl)-N'-ethylcarbodiimide and 2.5 ml of a 40 mM solution of N-hydroxysuccinimide, both prepared in buffer A, were added to the bead solution. The mixture was stirred for 20 min at room temperature. Next, activated beads were centrifuged at 4000 rpm for 5 min and washed once with 1 ml of 2 mM HCl. Beads were then resuspended in 1.5 ml of 20 mM Na_2HPO_4/NaH_2PO_4, pH 7.5 (buffer B) and 100 μl of serial dilutions of antibody or antigen in buffer B were added and left to react for 3 h at room temperature. Finally, conjugated beads were washed three times with 1 ml of buffer C (4000 rpm for 5 min) and stored in 250 μl of 20 mM Na_2HPO_4/NaH_2PO_4, 100 mM glycine, pH 7.5, with 3.3 mg/ml BSA and 0.02% NaN_3. In order to avoid multiple binding, the amount of coating antigen/antibody on the beads was tested at different concentrations until most unbinding events showed single rupture events. 100 μg of antibody and 250 μg of coating antigen per reaction showed the best results. The coupling efficiency of the immunoreagents to the polystyrene beads was checked by measuring the protein content of the supernatant after bioconjugation. In all cases the bioconjugation yield was between 85 and 90%, indicating a similar antibody/antigen density on the different biofunctionalized particles.

Antigens consist of low-weight/size estrogens (methyl-boldenone, 17β-boldenone and testosterone) linked to bovine serum albumin (BSA). Hapten design was carried out preserving the chemical, electronic and conformational properties of estrogens, while introducing a spacer arm for the covalent coupling to the BSA protein (Fig. 3a). Haptens were linked to BSA using the active ester method as previously described [1]. The use of BSA is mandatory to reduce electrostatic interactions between polystyrene beads.

S2 Optical tweezers setup

The optical tweezers instrument [2] consists of two counter-propagating infrared laser beams (845 nm) that form a single optical trap. Micron-sized beads can be captured and manipulated by optical gradient forces. By measuring the change of light momentum in the deflected beam using position-sensitive detectors (PSD) it is possible to directly measure the force applied to the bead. The position of the trap can be monitored using

piezoelectric actuators coupled to a wiggler device that bends the optical fiber of the lasers. The signal detected by the PSDs is processed by electronic microprocessors and data is sent to a computer and converted into forces and distances. The data acquisition frequency is 1 kHz, the force resolution is 0.1 pN and the distance resolution is 0.5 nm. All experiments are carried out in a microfluidics chamber that can be moved with a motorized stage. Temperature in the room is kept at 25±1^{o}C.

S3 Removal of multiple interactions

In order to remove multiple bonds that unbind simultaneously we use an extension of a statistical method proposed by Evans and collaborators[3] based on a Poissonian analysis of rupture forces: from a sample of N experiments we define the binding probability p as the ratio between the number of successful binding events to N. Next, the probability to find a given number x of parallel tethers is assumed to follow a Poisson distribution,

$$P(x) = \frac{e^{-\mu}\mu^x}{x!}. \tag{S1}$$

It can be shown that $\mu = -\log(1-p)$ and that the probability to find multiple bonds is equal to:

$$Q = P(x>1) = p - (p-1)\log(1-p). \tag{S2}$$

Therefore, $N \times Q$ gives an estimation of the number of simultaneous multiple binding events. Tables S1 and S2 show the number N of experiments, the number of successful binding events and the number of estimated simultaneous binding events $N \times Q$ for the different polyclonal and monoclonal interactions investigated.

Parallel tethers should dissociate at large forces. Moreover, the total stiffness measured in a pulling experiment is the sum of the different stiffnesses of each individual bond. Therefore, both large rupture forces and high stiffness values might suggest the presence of multiple tethers. We define the distance d:

$$d = \sqrt{\left(\frac{f_{\text{rupt}}}{f_{\text{rupt}}^{\text{max}}}\right)^2 + \left(\frac{k_{\text{bond}}}{k_{\text{bond}}^{\text{max}}}\right)^2}, \tag{S3}$$

where f_{rupt} and k_{bond} refer to rupture force and bond stiffness respectively, and $f_{\text{rupt}}^{\text{max}}$ and $k_{\text{bond}}^{\text{max}}$ are the respective maximum values experimentally measured. Finally, from the set of successful binding events, we remove the $N \times Q$ events with largest values of d.

bond	N	successful binding events	multiple bonds (eq. (S2))
Pab-MB-BSA	2674	1080	255
PreI-MB-BSA	1597	212	15
Pab-BSA	386	12	0
PreI-BSA	312	17	0

Table S1: **Polyclonal recognition and multiple binding events.** Number of experiments N, number of successful binding events, and estimated number of simultaneous multiple binding events according to the Poisson distribution.

bond	N	successful binding events	multiple bonds (eq. (S2))
Mab-B-BSA	2767	944	183
Mab-T-BSA	3347	756	93
Mab-BSA	2215	414	41

Table S2: **Monoclonal recognition and multiple binding events.** Number of experiments N, number of successful binding events, and estimated number of simultaneous multiple binding events according to the Poisson distribution.

S4 Bond stiffness

To quantify the flexibility of binding we measure the slope of experimental force-distance curves (denoted by k_{eff}) at the preset force value of 5 pN. k_{eff} contains the contributions of the rigidity of the antibody-antigen bond, k_{bond}, and the rigidity of the optical trap, $k_{\text{OT}} \simeq 0.078 \pm 0.005$ pN/nm[4]. The mathematical relation between the three different rigidities is given by:

$$\frac{1}{k_{\text{eff}}} = \frac{1}{k_{\text{bond}}} + \frac{1}{k_{\text{OT}}} \tag{S4}$$

$$k_{\text{bond}} = \frac{k_{\text{OT}} \cdot k_{\text{eff}}}{k_{\text{OT}} - k_{\text{eff}}}. \tag{S5}$$

S5 Removal of non-specific interactions

From pulling experiments carried out using Mab and the complex B-BSA we compute the 2D probability density function of bond stiffnesses (evaluated at 5 pN) and rupture forces, $p(k_{\text{bond}}, f_{\text{rupt}})$ (Fig. 3e in the main text). The set of measured unbinding events contains not only specific interactions between Mab and B, but also non-specific interactions between Mab and BSA. It is therefore important to remove the former interactions to properly characterize the thermodynamics and kinetics of the specific bond Mab-B. Several methods have been used for this purpose[5,6]. Most of them focus on one-dimensional analyses where only rupture forces are taken into account and bond rigidities

are neglected. Here we develop a 2-dimensional Bayesian inference method to extract the rupture force distributions of specific binding events, by including both $k_{\rm bond}$ and $f_{\rm rupt}$ in the analysis.

In terms of specific and non-specific binding events, $p(k_{\rm bond}, f_{\rm rupt})$ can be written as:

$$p(k_{\rm bond}, f_{\rm rupt}) = p(k_{\rm bond}, f_{\rm rupt}|B)p(B) + p(k_{\rm bond}, f_{\rm rupt}|BSA)p(BSA). \tag{S6}$$

where $p(B)$ and $p(BSA)$ are the probabilities of measuring binding to B or BSA respectively, and satisfy $p(B)+p(BSA) = 1$; $p(k_{\rm bond}, f_{\rm rupt}|B)$ and $p(k_{\rm bond}, f_{\rm rupt}|BSA)$ are the conditional probabilities of bond rigidities and rupture forces given the binding events Mab-B or Mab-BSA respectively.

The quantity $p(k_{\rm bond}, f_{\rm rupt}|BSA)$ can be measured experimentally by carrying out pulling experiments between Mab- and BSA-coated beads (Fig. 3e in the main text). However, pulling experiments between Mab- and B-coated beads are difficult due to the small size of B (see Methods in the main text). In order to evaluate $p(k_{\rm bond}, f_{\rm rupt}|B)$ we define a distance $I(k_0, f_0)$ between $p(k_{\rm bond}, f_{\rm rupt})$ and $p(k_{\rm bond}, f_{\rm rupt}|BSA)$ as:

$$I(k_0, f_0) = \int_0^{f_0} df_{\rm rupt} \int_0^{k_0} dk_{\rm bond} \;\; \left[p(k_{\rm bond}, f_{\rm rupt}) - p(k_{\rm bond}, f_{\rm rupt}|BSA)\right]^2 . \tag{S7}$$

The evaluation of $I(k_0, f_0)$ for the recognition between Mab and B is shown in Figure S1a. The profile of $I(k_0, f_0)$ shows a region (black area in the 2D contour plot, Fig. S1a) where we can assume that the probability $p(k_{\rm bond}, f_{\rm rupt}|B)$ of having specific binding Mab-B is negligible. Therefore, the probability of having non-specific binding events, $p(BSA) = 1 - P(B)$, can be derived from eq. (S6) as follows:

$$\int\int_{\text{black area}} df_{\rm rupt} dk_{\rm bond}\; p(k_{\rm bond}, f_{\rm rupt}) = \tag{S8}$$

$$= \underbrace{\int\int_{\text{black area}} df_{\rm rupt} dk_{\rm bond}\; p(k_{\rm bond}, f_{\rm rupt}|B)}_{=0}\, p(B) +$$

$$+ \int\int_{\text{black area}} df_{\rm rupt} dk_{\rm bond}\; p(k_{\rm bond}, f_{\rm rupt}|BSA)p(BSA) = \tag{S9}$$

$$= \int\int_{\text{black area}} df_{\rm rupt} dk_{\rm bond}\; p(k_{\rm bond}, f_{\rm rupt}|BSA)p(BSA) \tag{S10}$$

$$p(BSA) = \frac{\int\int_{\text{black area}} df_{\rm rupt} dk_{\rm bond}\; p(k_{\rm bond}, f_{\rm rupt})}{\int\int_{\text{black area}} df_{\rm rupt} dk_{\rm bond}\; p(k_{\rm bond}, f_{\rm rupt}|BSA)}. \tag{S11}$$

In the case under consideration, we get $p(BSA) = 0.90 \pm 0.05$.

Finally, using equation (S6) we obtain the probability $p(k_{\rm bond}, f_{\rm rupt}|B)$ associated only to specific binding events (Fig. S1b). In order to obtain the histogram of specific rupture forces we integrate over bond rigidities:

$$p(f_{\rm rupt}|B) = \int dk_{\rm bond}\ p(k_{\rm bond}, f_{\rm rupt}|B). \tag{S12}$$

In Figure S1c the histogram of specific rupture forces, $p(f_{\rm rupt}|B)$, obtained using the 2-dimensional Bayesian approach is shown (dotted curve). The histogram is also evaluated using other approaches where rigidity is not included, like plain subtraction of rupture force histograms, $p(f_{\rm rupt}) - p(f_{\rm rupt}|BSA)$ (dashed curve, Fig. S1d)[6], or setting a threshold force to separate specific from non-specific events (dotted curve, Fig. S1d)[5]. In the case of the specific interaction between Mab and B we see that different approaches give similar results.

The same procedure is carried out for the recognition between Mab and T. Results are shown in figure S2.

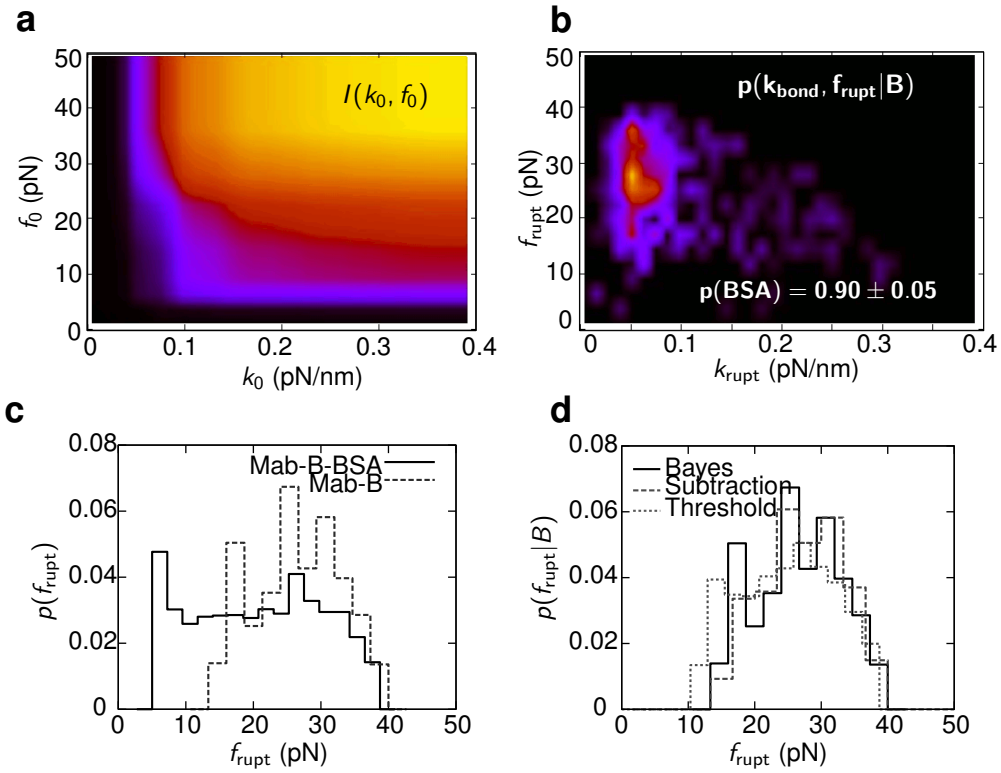

Figure S1: **Removal of non-specific interactions (related to Figure 4A). (a)** 2D contour plot of $I(k_0, f_0)$ (eq. (S7)) evaluated for the recognition events between Mab and the complex B-BSA. **(b)** 2D contour plot of specific recognition between Mab and B. **(c)** Rupture force histogram for the recognition events between Mab and the complex B-BSA (solid line) and for the specific recognition between Mab and B obtained with the Bayesian approach (dotted). **(d)** Specific rupture force histogram for the recognition between Mab and B, measured using equation (S12) (solid line); by subtracting rupture force histograms $p(f_{\rm rupt})$ and $p(f_{\rm rupt}|BSA)$ (dashed line)[6]; or by setting a threshold force to separate specific from non-specific events (dotted line)[5].

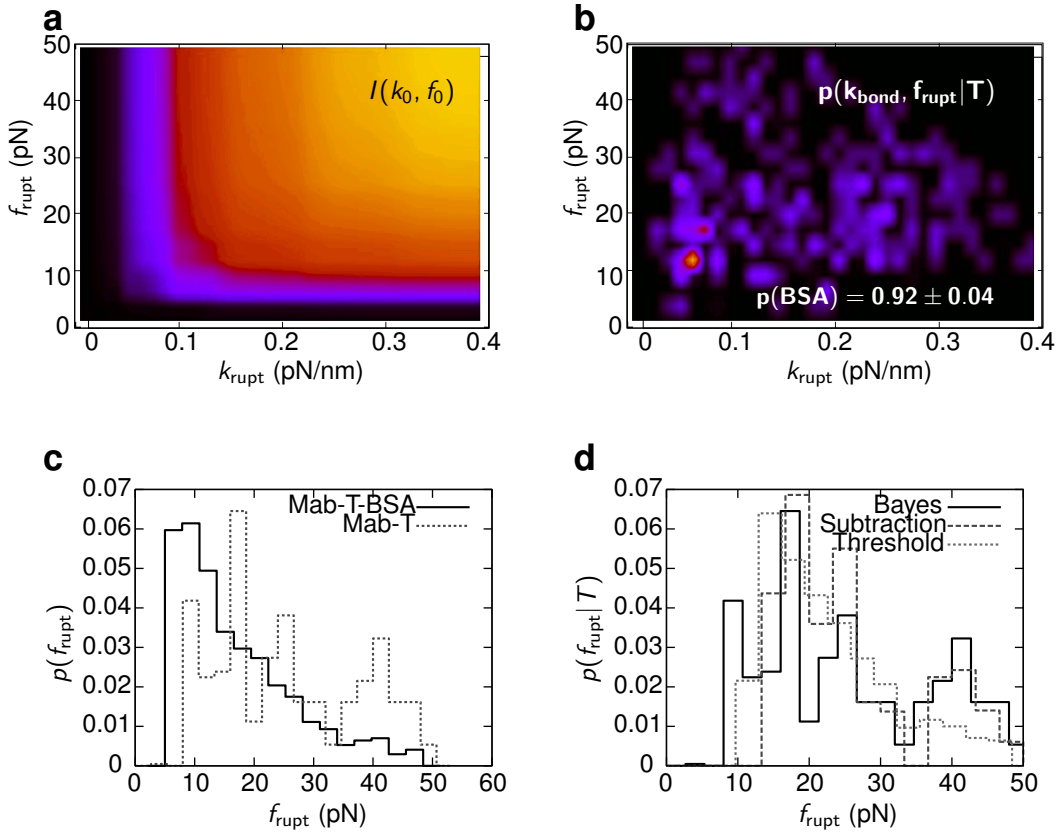

Figure S2: **Specific recognition between Mab and T (related to Figure 4B). (a)** 2D contour plot of $I(k_0, f_0)$ (eq. (S7)) evaluated for the recognition events between Mab and the complex T-BSA. **(b)** 2D contour plot of specific recognition between Mab and T. **(c)** Rupture force histogram for the recognition events between Mab and the complex T-BSA (black) and for the specific recognition between Mab and T obtained with the Bayesian approach (red). **(d)** Specific rupture force histogram for the recognition between Mab and T, measured using equation (S12) (red line); by subtracting rupture force histograms $p(f_{\rm rupt})$ and $p(f_{\rm rupt}|BSA)$ (green line)[6]; or by setting a threshold force to separate specific from non-specific events (blue line)[5].

S6 Force-induced breakage of molecular bonds

Mechanical bond dissociation is a statistical process that can be described with a master equation for the survival probability $P(f)$ (being the probability of the bond to remain intact at force f)[5,7,8]. For an applied force that increases linearly with time, $f(t) = rt$, the master equation is given by:

$$\frac{dP(f)}{df} = -\frac{k(f)}{v}P(f), \tag{S13}$$

where v is the loading rate in pN/s and $k(f)$ is the force-dependent rate of bond dissociation. It mostly depends on the shape of the free energy landscape (FEL) of the interaction[9]. Using a proper model for $k(f)$ it is possible to obtain key features of the FEL of the bond from force-spectroscopy measurements. Most well-accepted models are summarized below.

S6.1 Bell-Evans model

The simplest approach is given by the phenomenological Bell-Evans (BE) model[10], where $k(f)$ is equal to:

$$k(f) = k_0 \exp\left(\frac{fx^\dagger}{k_\mathrm{B}T}\right), \qquad k_0 = \omega_0 \exp\left(-\frac{\Delta G^\dagger}{k_\mathrm{B}T}\right). \tag{S14}$$

k_0 is the kinetic rate of bond dissociation at zero force; $\Delta G^\dagger$ the height of the kinetic barrier; $x^\dagger$ is the distance between the bonded and the transition state; k_B is the Boltzmann constant; and T is the temperature (taken equal to 298 K)[3,5,8,11]. The attempt rate of the bond ω_0 has been estimated previously for DNA and RNA hairpins, and values in the range $10^5 - 10^7$ s^{-1} have been obtained[12–14].

By introducing equation (S14) into (S13) we can analytically solve the resulting differential equation and obtain:

$$\log\left(-v \log P(f)\right) = \log\left(\frac{k_0 k_\mathrm{B}T}{x^\dagger}\right) + \log\left[\exp\left(\frac{fx^\dagger}{k_\mathrm{B}T}\right) - 1\right]. \tag{S15}$$

Next, by taking the derivative of $P(f)$ respect to force f we obtain an analytical expression for the probability density function of the rupture force, $p(f_\mathrm{rupt})$:

$$p(f_\mathrm{rupt}) = \frac{k_0}{v} \exp\left(\frac{f_\mathrm{rupt}x^\dagger}{k_\mathrm{B}T}\right) \exp\left\{-\frac{k_0 k_\mathrm{B}T}{vx^\dagger}\left[\exp\left(\frac{f_\mathrm{rupt}x^\dagger}{k_\mathrm{B}T}\right) - 1\right]\right\} \tag{S16}$$

Finally, using $p(f_{\text{rupt}})$ we can calculate the most probable rupture force $\langle f_{\text{rupt}} \rangle$ and the standard deviation σ_f, which in the case of the BE model are equal to:

$$\langle f_{\text{rupt}} \rangle = \frac{k_{\text{B}}T}{x^\dagger} \log\left(\frac{x^\dagger v}{k_0 k_{\text{B}} T}\right) \tag{S17}$$

$$\sigma_f = 0.96 \frac{k_{\text{B}}T}{x^\dagger} \tag{S18}$$

S6.2 Dudko-Hummer model

In the Dudko-Hummer (DH) model the kinetic rate $k(f)$ is evaluated from the Kramers theory of mean first passage times, which gives[15]:

$$k(f) = k_0 \frac{\int_{-\infty}^{x^\dagger} dx e^{\frac{-\Delta G(x) + fx}{k_{\text{B}}T}} \int_{-\infty}^{x} dy e^{\frac{\Delta G(y) - fy}{k_{\text{B}}T}}}{\int_{-\infty}^{x^\dagger} dx e^{\frac{-\Delta G(x)}{k_{\text{B}}T}} \int_{-\infty}^{x} dy e^{\frac{\Delta G(y)}{k_{\text{B}}T}}}, \tag{S19}$$

where k_0 is the kinetic rate of bond dissociation at zero force, $\Delta G(x)$ is the analytical expression of the FEL along the reaction coordinate x, and $x^\dagger$ is the position of the kinetic barrier. Therefore, by assuming an expression for $\Delta G(x)$ it is possible to compute $k(f)$.

In the Dudko-Hummer model the FEL is model with a single escape barrier located at $x^\dagger$. Two different mathematical expressions are proposed: the parabolic potential $\Delta G(x) = \Delta G^\dagger (x/x^\dagger)^2$ $(x < x^\dagger)$, or the cubic potential $\Delta G(x) = \frac{3}{2}\Delta G^\dagger x/x^\dagger - 2\Delta G^\dagger (x/x^\dagger)^3$ [16,17].

A unified expression for $k(f)$ can be obtained when solving equation (S19) with the aforementioned potentials:

$$k(f) = k_0 \left(1 - \gamma \frac{f x^\dagger}{\Delta G^\dagger}\right)^{1/\gamma - 1} \exp\left\{\frac{\Delta G^\dagger}{k_{\text{B}}T}\left[1 - \left(1 - \gamma \frac{f x^\dagger}{\Delta G^\dagger}\right)^{1/\gamma}\right]\right\}. \tag{S20}$$

γ is a parameter related to the shape of the FEL: $\gamma = 1/2$ corresponds to the parabolic potential whereas $\gamma = 2/3$ corresponds to the cubic potential. For $\gamma = 1$ the expression from the Bell-Evans model (eq. (S14)) is recovered.

Again, the differential equation obtained by introducing equation (S20) into (S13) can be analytically solved:

$$\log\left(-v \log P(f)\right) = \log\left(\frac{k_0}{x^\dagger}\right) + \log\left\{\exp\left[\frac{\Delta G^\dagger}{k_{\text{B}}T}\left(1 - \left(1 - \gamma \frac{f x^\dagger}{\Delta G^\dagger}\right)^{1/\gamma}\right)\right] - 1\right\}. \tag{S21}$$

From the derivative of $P(f)$ as a function of force we get the probability density

function of the rupture force, $p(f_{\rm rupt})$:

$$p(f_{\rm rupt}) = \frac{k_0}{v}\left(1-\gamma\frac{f_{\rm rupt}x^\dagger}{\Delta G^\dagger}\right)\exp\left\{\frac{\Delta G^\dagger}{k_{\rm B}T}\left[1-\left(1-\gamma\frac{f_{\rm rupt}x^\dagger}{\Delta G^\dagger}\right)^{1/\gamma}\right]-\right.$$
$$\left.-\frac{k_0 k_{\rm B}T}{vx^\dagger}\left(e^{\frac{\Delta G^\dagger}{k_{\rm B}T}\left[1-\left(1-\gamma\frac{f_{\rm rupt}x^\dagger}{\Delta G^\dagger}\right)^{1/\gamma}\right]}-1\right)\right\}. \tag{S22}$$

Finally, we can calculate the most probable rupture force $\langle f_{\rm rupt}\rangle$ and the standard deviation σ_f:

$$\langle f_{\rm rupt}\rangle = \frac{\Delta G^\dagger}{\gamma x^\dagger}\left\{1-\left[\frac{k_{\rm B}T}{\Delta G^\dagger}\log\left(\frac{k_0 k_{\rm B}T e^{\frac{\Delta G^\dagger}{k_{\rm B}T}+0.577}}{x^\dagger v}\right)\right]^\gamma\right\} \tag{S23}$$

$$\sigma_f = \frac{k_{\rm B}T\pi}{\sqrt{6}x^\dagger}\left[\frac{k_{\rm B}T}{\Delta G^\dagger}\log\left(\frac{k_0 k_{\rm B}T e^{\frac{\Delta G}{k_{\rm B}T}+1.064}}{x^\dagger v}\right)\right]^{\gamma-1} \tag{S24}$$

S7 Force spectroscopy analysis

Taking into account that the FEL of the Mab-B bond can be described with a single escape barrier we performed a more detailed analysis of rupture forces. We carry out pulling experiments between Mab-coated beads and B-BSA-coated beads at three different pulling speeds (v ∼20, 70 and 140 nm/s) and remove non-specific interactions that take place between Mab and BSA (Section S5). In figure S3 we show the obtained histograms of $f_{\rm rupt}$ (panel a), most probable rupture forces $\langle f_{\rm rupt}\rangle$ and standard deviations σ_f as a function of the pulling speed v (panel b, top and bottom respectively). Using equations (S17) and (S18) for the BE model and equations (S23) and (S24) for the DH model simultaneous fits can be carried out to both magnitudes. Results, shown in Figure S3 (right) and summarized in Table S3, are in good agreement within error bars with previous estimations (Table 1).

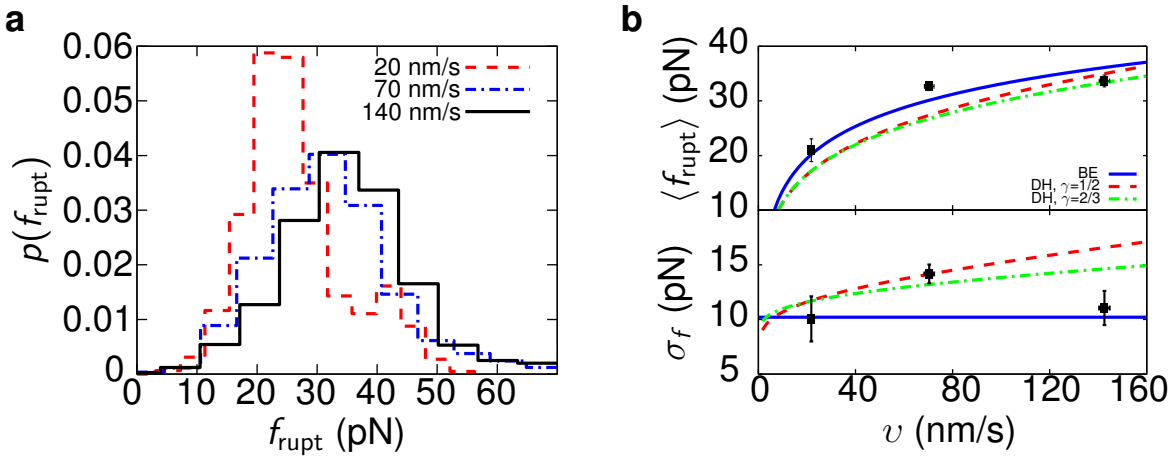

Figure S3: **Pulling and force jump experiments for the specific bond Mab-B. (a)** Pulling rate dependence of the specific rupture force histogram for the interaction Mab-B measured in pulling experiments (left) **(b)** loading rate dependence of the average rupture forces (right top) and standard deviations (right bottom) for Mab-B. Simultaneous fits using the BE (solid blue line) and the DH (dashed red for γ=1/2 and dashed-dotted green for γ=2/3) models (Supplementary Information, section S1)

Table S3: **Free-energy landscape parameters for Mab-B.** Estimations of $x^\dagger$, k_0 and $\Delta G^\dagger$ obtained from pulling experiments using the BE and the DH fits of $\langle f_{\rm rupt} \rangle$ and σ_f as a function of the pulling speed v (Fig. S3b).

FEL model	$x^\dagger$ (Å)	k_0 (s^{-1})	$\Delta G^\dagger$ (k_BT)
BE	5.0±0.3	0.008±0.002	–
Parabolic	8.0±1.0	0.0002±0.0001	13±4
Cubic	7.0±1.0	0.0002±0.0001	12±3

References

(1) Estévez, M.-C.; Galve, R.; Sánchez-Baeza, F.; Marco, M.-P. *Anal. Chem.* **2005,** *77*, 5283–5293.

(2) Huguet, J. M.; Bizarro, C. V.; Forns, N.; Smith, S. B.; Bustamante, C.; Ritort, F. *Proc. Natl. Acad. Sci. USA* **2010,** *107*, 15431–15436.

(3) Evans, E.; Kinoshita, K.; Simon, S.; Leung, A. *Biophys. J.* **2010,** *98*, 1458–1466.

(4) Forns, N.; De Lorenzo, S.; Manosas, M.; Hayashi, K.; Huguet, J.; Ritort, F. *Biophys. J.* **2011,** *100*, 1765–1774.

(5) Evans, E.; Halvorsen, K.; Kinoshita, K.; Wong, W. *Handbook of Single Molecule Biophysics;* Springer Science+Business Media, LLC 2009; 571–589.

(6) Wagner, C.; Singer, D.; Ueberschär, O.; Stangner, T.; Gutsche, C.; Hoffmann, R.; Kremer, F. *Soft Matter* **2011,** *7*, 4370–4378.

(7) Simson, D.; Strigl, M.; Hohenadl, M.; Merkel, R. *Phys. Rev. Lett.* **1999,** *83*, 652–655.

(8) Strigl, M.; Simson, D. A.; Kacher, C. M.; Merkel, R. *Langmuir* **1999,** *15*, 7316–7324.

(9) Strunz, T.; Oroszlan, K.; Schumakovitch, I.; Güntherodt, H.-J.; Hegner, M. *Biophys. J.* **2000,** *79*, 1206–1212.

(10) Bell, G. I. *Science* **1978,** *200*, 618–627.

(11) Merkel, R.; Nassoy, P.; Leung, A.; Ritchie, K.; Evans, E. *Nature* **1999,** *397*, 50–53.

(12) Manosas, M.; Collin, D.; Ritort, F. *Phys. Rev. Lett.* **2006,** *96*, 218301.

(13) Engel, S.; Alemany, A.; Forns, N.; Maass, P.; Ritort, F. *Philos. Mag.* **2011,** *91*, 2049–2065.

(14) Bizarro, C. V.; Alemany, A.; Ritort, F. *Nucleic Acids Res.* **2012,** *40*, 6922–6935.

(15) Kramers, H. A. *Physica* **1940,** *7*, 284–304.

(16) Dudko, O. K.; Hummer, G.; Szabo, A. *Phys. Rev. Lett.* **2006,** *96*, 108101.

(17) Dudko, O. K.; Hummer, G.; Szabo, A. *Proc. Natl. Acad. Sci. USA* **2008,** *105*, 15755–15760.